Enhanced magnetoelectric properties of $BiFeO_3$ on formation of $BiFeO_3/SrFe_{12}O_{19}$ nanocomposites

Anusree Das, Souvik Chatterjee, Sudipta Bandyopadhyay, and Dipankar Das'

Citation: J. Appl. Phys. **119**, 234102 (2016); doi: 10.1063/1.4954075
View online: http://dx.doi.org/10.1063/1.4954075
View Table of Contents: http://aip.scitation.org/toc/jap/119/23
Published by the American Institute of Physics

Enhanced magnetoelectric properties of $BiFeO_3$ on formation of $BiFeO_3/SrFe_{12}O_{19}$ nanocomposites

Anusree Das,[1] Souvik Chatterjee,[1] Sudipta Bandyopadhyay,[2] and Dipankar Das[1,a)]
[1]*UGC-DAE Consortium for Scientific Research, Kolkata Centre, III/LB-8, Bidhannagar, Kolkata 700098, India*
[2]*Department of Physics, University of Calcutta, Kolkata 700009, India*

(Received 10 February 2016; accepted 4 June 2016; published online 17 June 2016)

Nanocomposites (NCs) comprising $(1-x)$ $BiFeO_3$ (BFO) and x $SrFe_{12}O_{19}$ (SRF) ($x = 0.1$, 0.2, 0.3, and 0.4) have been prepared by a sol-gel route. Presence of pure phases of both $BiFeO_3$ (BFO) and $SrFe_{12}O_{19}$ (SRF) in the NCs for $x = 0.3$ and 0.4 has been confirmed by Rietveld analysis of XRD data though a minor impurity phase is observed in the case of $x = 0.1$ and 0.2 NCs. Transmission electron micrographs of the NCs show that particles are mostly spherical with average size of 30 nm. M-H measurements at 300 and 10 K indicate predominantly ferrimagnetic behavior of all the NCs with an increasing trend of saturation magnetization values with increasing content of SRF. Dielectric constant (ε_r) of the NCs at room temperature shows a dispersive behavior with frequency and attains a constant value at higher frequency. $\varepsilon_r - T$ measurements reveal an increasing trend of dielectric constant of the NCs with increasing temperature and show an anomaly around the antiferromagnetic transition temperature of BFO, which indicates magnetoelectric coupling in the NCs. The variation of capacitance in the presence of magnetic field confirms the enhancement of magnetoelectric effect in the NCs. ^{57}Fe Mössbauer spectroscopy results indicate the presence of only Fe^{3+} ions in usual crystallographic sites of BFO and SRF. *Published by AIP Publishing.*
[http://dx.doi.org/10.1063/1.4954075]

I. INTRODUCTION

Multiferroics are materials with two or more primary ferroic properties such as ferroelasticity, ferroelectricity, and ferro/ferri-magnetism that are united in the same phase and have drawn considerable attention of research community recently due to their potential applications in spintronics, memory devices, electromagnetic sensors, etc.[1] Multiferroics exhibit magnetoelectric (ME) effect that enables one to tune electric polarization by application of external magnetic field or induce magnetization by electric field in these classes of materials.[2] Bismuth ferrite ($BiFeO_3$, BFO) having high ferroelectric (Curie temperature, $T_C \sim 1103$ K) and antiferromagnetic (Neel temperature, $T_N \sim 643$ K) transition temperatures[3] is one of the most studied multiferroics because it shows magnetoelectric (ME) coupling effect at room temperature and hence is a potential candidate for future technological applications. But magnetoelectric coupling coefficient of bismuth ferrite (BFO) is rather weak that is primarily due to large leakage current caused by the presence of oxygen vacancies.[4] In addition, being a G-type antiferromagnet with spiral spin structure, BFO gives weak ferromagnetic hysteresis loop with low saturation magnetization. Improvement of ferroelectric and magnetic properties of BFO can be achieved either by proper substitution of suitable elements in the required site or by making a composite of BFO with another compound.[5–9] This compound should have good ferroelectric and/or ferromagnetic properties that can enhance the desired properties of BFO along with the improvement in magnetoelectric coupling.

In the present work, strontium hexaferrite ($SrFe_{12}O_{19}$, SRF), a ferrimagnetic material with high magnetic moment, has been chosen as the compound to be associated with BFO. In an earlier work, we have reported magnetic and hyperfine properties of BFO-SRF nanocomposite (NC) with 30 M % of SRF.[10] In the present paper, nanocomposites of bismuth ferrite (BFO) and strontium hexaferrite (SRF) with 10 to 40 M % of SRF have been prepared by the sol-gel method. Structural, magnetic, dielectric, and magnetodielectric properties of the nanocomposites have been investigated to establish the role of SRF in enhancing magnetic and dielectric properties of BFO. A clear signature of improvement of magnetic as well as magnetodielectric properties of the NCs with respect to the pristine BFO has been noticed, which has not been reported earlier.

II. EXPERIMENTAL DETAILS

Nanocomposites with chemical formula x $SrFe_{12}O_{19}$-$(1-x)$ $BiFeO_3$ with x varying from 0.1 to 0.4 have been prepared by adopting a chemical sol-gel route.[11] Stoichiometric amounts of iron (III) nitrate nonahydrate ($Fe(NO_3)_3{\cdot}9H_2O$), bismuth nitrate pentahydrate ($Bi(NO_3)_3{\cdot}5H_2O$), strontium nitrate ($Sr(NO_3)_2$), and citric acid were weighed. First, citric acid was dissolved in minimum amount of distilled water. Then, weighed salts were successively added to the acid solution with continuous stirring. Next, appropriate amount of ethylene glycol was added to the resultant solution such that the mass ratio of citric acid to ethylene glycol became 3:2. Ethylene glycol helped to get a homogeneous solution and uniform particle size distribution, whereas citric acid in the present case acted as a chelating agent. The transparent brownish solution thus obtained was heated at 373 K

a)Email: ddas@alpha.iuc.res.in

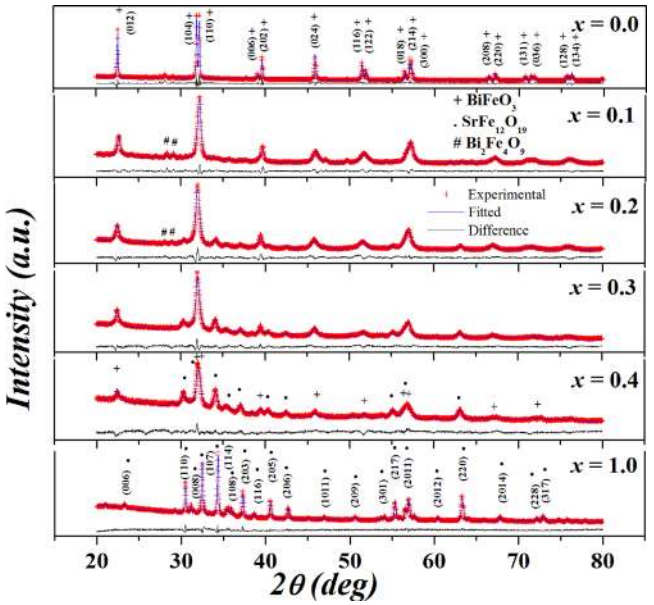

FIG. 1. Room temperature XRD patterns of all pristine samples and nanocomposites.

with continuous stirring until a viscous gel had developed. The obtained gel was dried thoroughly under an IR lamp. After an hour, the gel turned into a fluffy mass that was crushed in an agate mortar. The as-prepared gel powder was annealed at 873 K for 2 h to obtain the desired crystalline phase.

Prepared samples were characterized by x-ray diffraction (XRD), Mössbauer spectroscopy, SQUID magnetometry, and magnetoelectric measurements. To identify the crystalline phases present in the samples, x-ray diffractograms were recorded using a Bruker D8 Advance x-ray diffractometer with a Cu Kα radiation (wavelength = 1.5406 Å) source operated at 40 mA and 40 kV. Morphological studies and particle size distribution of the samples had been carried out using a high resolution transmission electron microscope (TEM) (JEOL 2100) working at 200 kV. ^{57}Fe Mössbauer spectroscopic studies had been carried out using a pc-based 1024 channel multichannel analyzer supplied by Wissel GmbH, Germany, operating in the constant acceleration mode. A 25mCi ^{57}Co source in Rh matrix was used as the radioactive source, and all measurements were taken in the transmission geometry. The spectrometer was calibrated with a 12 μm thick pure natural iron foil, and all isomer shifts are measured with respect to the centroid of the sextet pattern of the natural iron foil. DC magnetization measurements had been performed using a SQUID magnetometer (MPMS XL 7, Quantum Design, USA). Room temperature magnetoelectric measurements have been performed using a cryogen-free high magnetic field (15 T) system (from Cryogenic, UK) coupled to a Keysight E4980A Precision LCR meter. High temperature dielectric measurements have been done using an Agilent E4980A Precision LCR meter.

III. RESULTS AND DISCUSSION

A. X-ray diffraction studies

Structural parameters and purity of the phases present in the prepared nanocomposites were determined by x-ray diffraction analysis. Fig. 1 shows x-ray diffraction (XRD) patterns of the pristine and all nanocomposite samples. The observed peaks correspond to reflections from crystal planes of both perovskite $BiFeO_3$ (JCPDS Card No. 86-1518) and hexagonal $SrFe_{12}O_{19}$ (JCPDS Card No. 79-1411). Presence of two ferrite phases confirms successful formation of the composite. For the NCs with $x = 0.1$ and 0.2, some additional peaks are seen that have been identified as due to $Bi_2Fe_4O_9$ phase (JCPDS Card No. 74-1098). Area percentages of this impure phase are approximately 11% and 5% for $x = 0.1$ and 0.2, respectively. Intensities of peaks due to SRF phase are seen to increase with the increment of SRF content in the nanocomposite as expected. It is also evident from the figure that the amount of the impurity phase reduces with the increase of SRF content in the NCs[9] and finally becomes untraceable at $x = 0.3$. Structural parameters and particle sizes of the phases present in all the samples are obtained by the Rietveld refinement analysis of XRD patterns using the MAUD software.[12] Analyzed parameters are given in Table I. It can be seen from Table I that particle sizes of both BFO and SRF in the NCs are much lower than that of the pristine BFO and pristine SRF. This indicates restricted grain growth of both the constituents during the formation of the NCs. The obtained particle sizes of BFO are 40, 31, 30, and 36 nm and that of SRF are 17, 23, 21, and 20 nm for $x = 0.1$, 0.2, 0.3, and 0.4, respectively. Twin peaks of BFO such as (104), (110); (006), (202); (116), (122); and (018), (214) are found to merge together giving a single broadened peak in all nanocomposites. Similar merging had been reported in doped BFO samples by others[13,14] that were assigned to structural distortion. The merging of twin peaks of BFO in the present case indicates distortion of rhombohedral structure of BFO as BFO-SRF composite forms. It is also seen from the patterns that diffraction peaks of BFO in NCs are slightly shifted to lower angles with increasing content of SRF. This shifting denotes gradual increment in lattice parameters of BFO with incorporation of increasing

TABLE I. Fitted parameters of XRD data for x $SrFe_{12}O_{19}$-$(1-x)$ $BiFeO_3$ nanocomposites.

Value of x	a value of BFO (Å)	c value of BFO (Å)	a value of SRF (Å)	c value of SRF (Å)	Particle size of BFO (nm)	Particle size of SRF (nm)
0.0	5.5832	13.8834	…	…	537	…
0.1	5.6025	13.7173	5.8981	22.5657	40	17
0.2	5.5938	13.7062	5.8846	23.3279	31	23
0.3	5.5896	13.6878	5.8885	23.1959	30	21
0.4	5.5969	13.6768	5.8936	23.1934	36	21
1.0	…	…	5.8880	23.0825	…	147

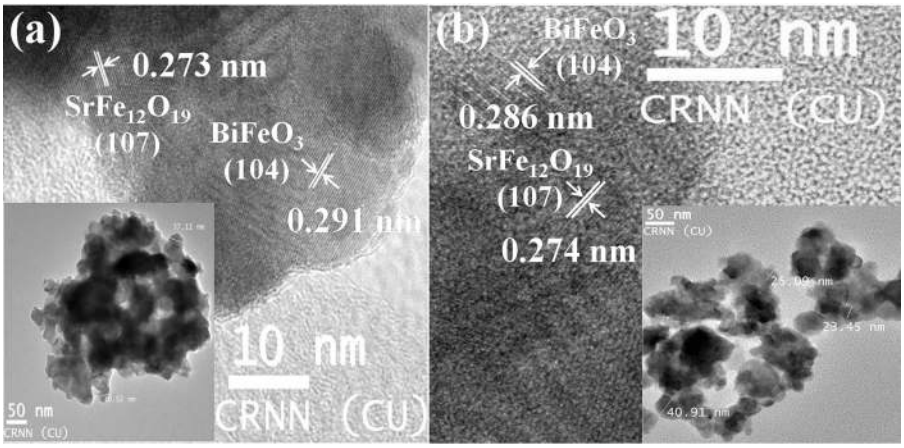

FIG. 2. HRTEM image of (a) 0.3SRF-0.7BFO NC and (b) 0.4SRF-0.6BFO NC. Insets show TEM images of the same samples.

SRF content in the NCs. Similar shift has been reported by others also.[9,15]

B. TEM studies

The morphology and size distribution of the particles in the NCs are studied by transmission electron microscopy (TEM). Insets of Figs. 2(a) and 2(b) show TEM micrographs of NCs with $x = 0.3$ and 0.4, respectively, whereas the main panels exhibit high resolution TEM images of the same samples. From the TEM images, it can be seen that the particles are mostly spherical and are uniformly distributed. Average particle sizes of the constituents are around 30 and 32 nm for $x = 0.3$ and 0.4 NCs, respectively, and these particle sizes agreed well with XRD results. The high resolution image of 0.3SRF-0.7BFO NC (Fig. 2(a)) depicts two types of lattice fringes with fringe width of 0.291 and 0.273 nm, whereas high resolution image of 0.4SRF-0.6BFO NC (Fig. 2(b)) shows lattice fringes with widths 0.286 and 0.274 nm. These widths are close to the reported d spacing values for the (104) and (107) crystal planes of BFO and SRF, respectively (JCPDS Card Nos. 86-1518 and 79-1411, respectively). Presence of crystal planes corresponding to most intense peaks of both BFO and SRF confirms successful formation of the composite with nanometer scaled particle size.

C. Magnetic studies

Magnetic properties of the samples were studied by a SQUID magnetometer. Fig. 3 shows magnetic hysteresis loops (M-H) of all nanocomposites recorded at room temperature, whereas the inset shows the same for the pristine BFO at room temperature. It is clearly seen from Fig. 3 that magnetic moments of the nanocomposite samples are substantially higher than that of the pristine BFO. It can be noted that there is a small impure phase of $Bi_2Fe_4O_9$ present in the NCs for $x = 0.1$ and 0.2. But $Bi_2Fe_4O_9$ is paramagnetic at room temperature, so it has negligible contribution to the measured magnetization value of those NCs. It is also evident from Fig. 3 that the values of saturation magnetization (M_s) and remnant magnetization (M_r) of the composites increase with the increment of x value. It is known that BFO with size less than ~62 nm is weakly ferromagnetic and SRF is ferrimagnetic in nature. Converting the molar percentages of SRF and BFO in the NCs to weight percentages and taking saturation magnetization value of pure SRF sample as 66.3 emu/g and pure BFO as 0.5 emu/g (Table II), the saturation magnetization values of the NCs with $x = 0.1$, 0.2, 0.3, and 0.4 were estimated to be 18.56, 30.77, 39.60, and 46.15 emu/g, respectively. But the measured saturation magnetization values of the NCs with $x = 0.1$, 0.2, 0.3, and 0.4 are 15.1, 27.3, 37.2, and 48.1, respectively (Table II). This difference between the estimated and experimentally measured values clearly demonstrates that net magnetization of the NCs is not merely the sum of the contributions from their components. For the NCs with $x = 0.1$, 0.2, and 0.3, the measured M_s values are slightly less, whereas for $x = 0.4$, it is slightly more than the estimated values. This may be explained by considering the dipolar interaction between magnetic moments of BFO and SRF across the interfaces as they are in close contact in the NCs. For the NCs with $x = 0.1$, 0.2, and 0.3 as fraction of BFO is more than that of SRF, the effective magnetic moment of SRF is reduced by antiferromagnetic BFO dipoles located near the interfaces and hence net magnetization of the NCs is reduced. As the fraction of SRF increases ($x = 0.4$) in the NC, the field created by dipole moments of SRF overrides the negative effect of BFO as explained above and align dipole moments of

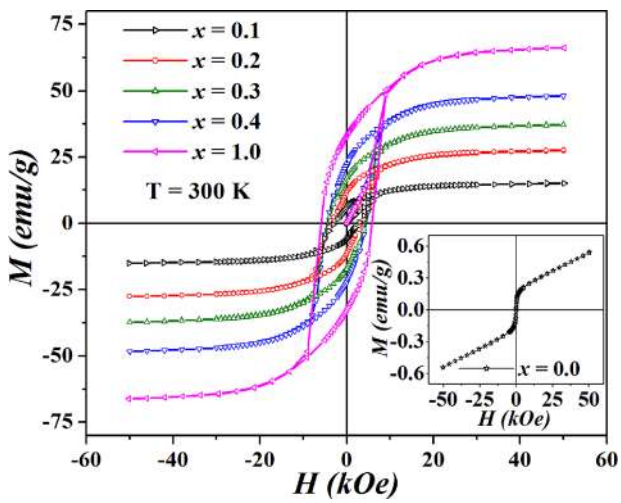

FIG. 3. Room temperature magnetic hysteresis loops of the pristine SRF and all nanocomposites. Inset shows room temperature hysteresis loop of the pristine BFO NPs.

TABLE II. Magnetic parameters of x $SrFe_{12}O_{19}$-$(1-x)$ $BiFeO_3$ nanocomposites.

x value	Measuring temperature (K)	M_s at 50 kOe (emu/g)	M_r (emu/g)	H_c (Oe)
0.0	300	0.5	0.02	68
	10	0.8	0.1	874
0.1	300	15.1	6.1	2798
	10	20.7	10.2	4166
0.2	300	27.3	11.6	3618
	10	41.1	21.1	5256
0.3	300	37.2	17.2	4328
	10	54.3	28.1	5746
0.4	300	48.1	22.2	4483
	10	68.0	35.1	5930
1.0	300	66.3	32.9	5793

BFO parallel to SRF moments causing a net increase of magnetization. Similar enhancement of magnetization of a NC due to interfacial strain has been reported by others also.[16] From the M-H loops (Fig. 3), it is also seen that the coercivity (H_c) of the nanocomposites increases with the increasing content of SRF. This enhancement in H_c could be due to complexity of having two different magnetic spin components (BFO and SRF) in the composites that increases anisotropy energy of the system. Fig. 4 represents M-H hysteresis loops of all nanocomposites recorded at 10 K, and the inset shows the hysteresis loop of the pristine BFO taken at the same temperature. The M_s, M_r, and H_c values of nanocomposites get increased at low temperature. The increase in M_s and M_r values is assigned to the decrement of thermal fluctuation of magnetic spins at lower temperature and their alignment in the applied field direction. The increment of H_c value on lowering of temperature is attributed to freezing of surface spins that requires higher magnetic field to demagnetize the sample.

D. Dielectric studies

Frequency dependent dielectric constant (ε_r) curves recorded at room temperature of all nanocomposites and the pristine BFO are shown in Fig. 5. Dielectric constant decreases with increasing frequency and finally becomes constant at higher frequency region for all samples. Electric dipoles are able to follow the frequency of applied electric field in the low frequency region that causes larger value of ε_r, but at higher frequency, dipoles are not able to follow the electric field giving lower value of ε_r.[14] It can be seen from Fig. 5 that ε_r values have decreased in the composites in comparison with that of the pristine BFO. This indicates degradation in dielectric properties of the composites with addition of SRF. Fig. 6 shows the variation of dielectric constant (ε_r) of all nanocomposites and the pristine BFO with temperature in the region 300–773 K. The inset shows temperature dependence of dielectric loss ($\tan\delta$) in the same temperature range. Both ε_r and $\tan\delta$ values increase with increase in temperature. One large anomaly is observed in all samples near 702 K in both ε_r-T and $\tan\delta$-T graphs. It is known that bulk BFO exhibits antiferromagnetic transition around 643 K. The anomaly seen around 702 K is in the vicinity of antiferromagnetic Neel temperature of BFO.[17,18] Signature of a magnetic transition in the temperature dependent dielectric

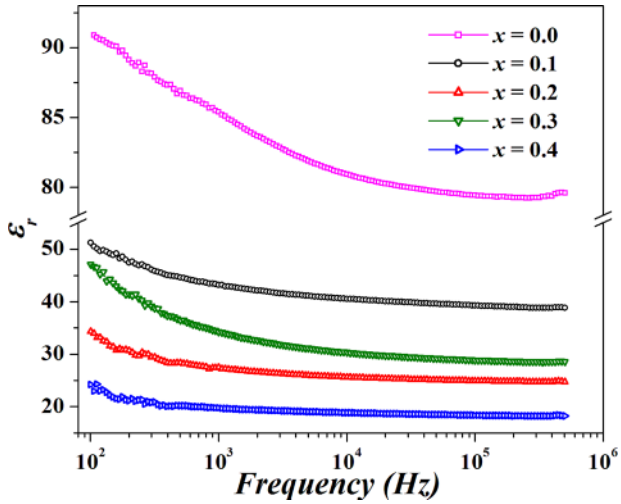

FIG. 5. Frequency dependent dielectric constant curves of all prepared samples at room temperature.

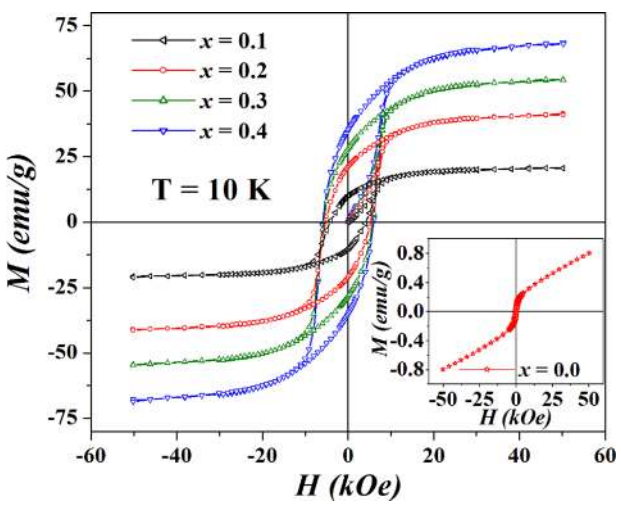

FIG. 4. Magnetic hysteresis loops of all NCs at 10 K. Inset exhibits the same of the pristine BFO.

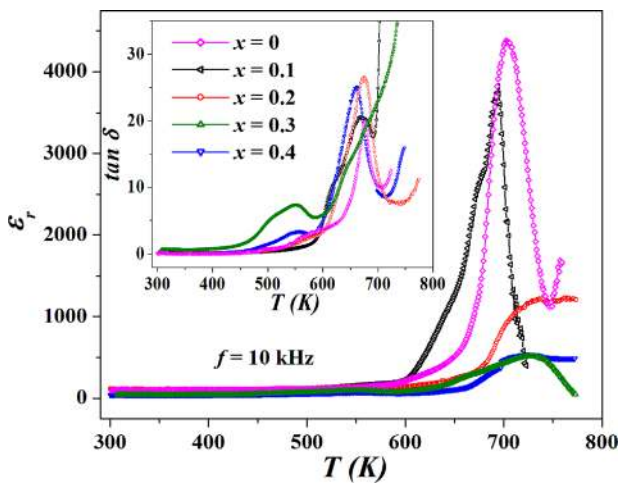

FIG. 6. Temperature dependence of dielectric constant and dielectric loss (inset) of all samples.

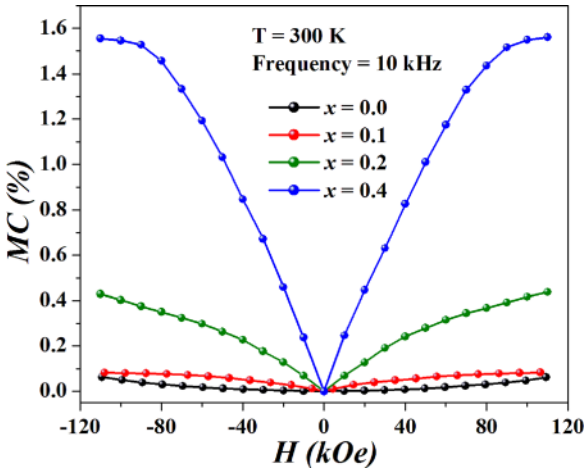

FIG. 7. Magnetic field-induced change in dielectric constant at 10 kHz of the pristine BFO and NCs ($x = 0.1$, 0.2, and 0.4) measured at 300 K.

constant curves indicates orientation of magnetic dipole moments of BFO in the presence of external electric field, i.e., magnetoelectric coupling in all NCs along with the pristine BFO. It is also seen from Fig. 6 that the magnitude of this anomaly (peak intensity) reduces with the increase in SRF content, which is attributed to the presence of higher fraction of the ferrimagnetic component that suppresses the effect of antiferromagnetic BFO. Another anomaly is observed around 550 K in temperature dependent dielectric constant and dielectric loss curves of NCs with $x = 0.2$, 0.3, and 0.4. Similar anomaly has been observed in BFO near 450 K, which is assigned to the Fe^{3+}/Fe^{2+} charge transfer.[14,19] But in our samples, no such anomaly is found in the pristine BFO. The anomaly observed in present three NCs near 550 K is attributed to hopping of electrons between Fe^{2+} and Fe^{3+} ions at the octahedral sites of $SrFe_{12}O_{19}$. The crystal structure of SRF is hexagonal and Fe ions occupy tetrahedral, octahedral, and trigonal bipyramidal sites. Fe^{2+} ions formed during annealing of the as- prepared sample prefer to go to the octahedral sites.[20] In the pristine BFO, this anomaly is absent and in 0.1SRF-0.9BFO NC, it was not detected due to low content of SRF. With the increment of SRF content, the anomaly becomes more prominent.

E. Magnetoelectric studies

Magnetoelectric (ME) coupling facilitates tailoring of magnetic properties in the presence of electric field and the tuning of electric properties by applying the external magnetic field of multiferroic materials. Magnetocapacitance (MC) is a measure of the change in dielectric constant of a material in the presence of magnetic field and therefore is a parameter to test the presence of magnetoelectric effect. Magnetocapacitance is defined as $MC = [\varepsilon_r(H) - \varepsilon_r(0)]/\varepsilon_r(0)$, where $\varepsilon_r(H)$ and $\varepsilon_r(0)$ denote dielectric constants at applied field H and zero field, respectively.[21] In multiferroics, both ferroelectricity and ferromagnetism are present in a single phase. It is known that

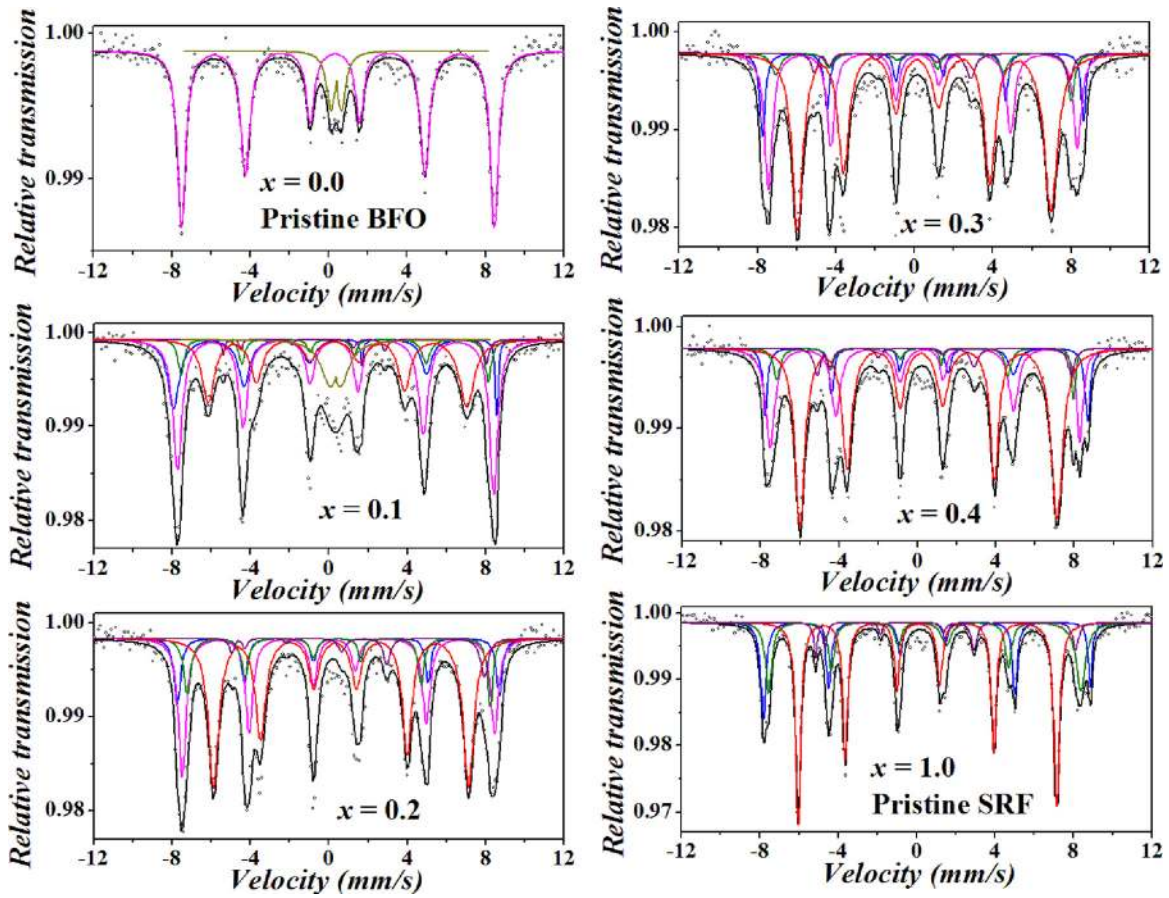

FIG. 8. Room temperature Mössbauer spectra of all samples (open circles: experimental, black: fitted, blue: $4f_2$, green: 2a and $4f_1$, red: 12 k, purple: 2b, magenta: BFO, dark yellow: $Bi_2Fe_4O_9$).

TABLE III. Mössbauer hyperfine parameters of x $SrFe_{12}O_{19}$-$(1-x)$ $BiFeO_3$ nanocomposites.

x value	Site	Isomer shift (mm/s)	Quadrupole splitting (mm/s)	Line width (mm/s)	Internal hyperfine field (kOe)
0.0	BFO	0.38	0.14	0.53	496
	$Bi_2Fe_4O_9$	0.38	0.52	0.56	…
0.1	12 k	0.27	0.36	0.78	410
	$4f_2$	0.33	0.01	0.51	512
	$4f_1+2a$	0.24	0.03	0.38	487
	2b	0.07	2.15	0.24	417
	BFO	0.28	0.12	0.54	501
	$Bi_2Fe_4O_9$	0.33	0.49	1.1	…
0.2	12 k	0.40	0.36	0.62	404
	$4f_2$	0.43	0.10	0.37	510
	$4f_1+2a$	0.38	0.29	0.39	480
	2b	0.03	2.16	0.38	400
	BFO	0.41	0.03	0.47	495
0.3	12 k	0.26	0.38	0.70	402
	$4f_2$	0.27	0.34	0.30	508
	$4f_1+2a$	0.24	0.35	0.49	468
	2b	0.09	2.15	0.43	404
	BFO	0.30	0.11	0.49	489
0.4	12 k	0.32	0.39	0.62	407
	$4f_2$	0.35	0.19	0.34	511
	$4f_1+2a$	0.22	0.30	0.34	470
	2b	0.07	2.15	0.41	402
	BFO	0.32	0.01	0.51	491
1.0	12 k	0.27	0.40	0.32	410
	$4f_2$	0.37	0.25	0.29	518
	$4f_1+2a$	0.29	0.24	0.43	495
	2b	0.13	2.34	0.27	412

ferroelectrics are also piezoelectrics, i.e., they become electrically polarized under an applied stress. In a multiferroic, application of external magnetic field results a strain. This strain induces stress in the material (as it is piezoelectric) that creates an electric field.[22] In the presence of the electric field, ferroelectric domains of the sample align themselves in field direction and enhance polarization and hence modify dielectric constant of the sample. Fig. 7 represents variation of magnetocapacitance of nanocomposites for compositions $x=0.1$, 0.2, and 0.4 and the pristine BFO measured at 10 kHz in the presence of magnetic field ranging from −110 to 110 kOe. It is evident from the figure that all curves in positive and negative field regions are mostly symmetric about the zero field axis. With the increment of external magnetic field, magnetocapacitance of all samples increases indicating a positive magnetoelectric effect. It can be seen from the figure that MC of the NCs increases with the increasing content of SRF and becomes substantially high in the case of the NC with $x=0.4$. MC values of the samples are found to be 0.06%, 0.08%, 0.44%, and 1.56% at 110 kOe for the pristine BFO ($x=0.0$) and NCs with $x=0.1$, 0.2, and 0.4, respectively. This enhancement of MC is attributed to the stronger coupling between magnetic and ferroelectric domains[21] due to the presence of ferrimagnetic domains of SRF next to antiferromagnetic BFO, which increases magnetic moment of the composite system and hence MC through the magnetoelectric coupling. As $Bi_2Fe_4O_9$ is paramagnetic at room temperature, it cannot be multiferroic at that temperature. Hence, $Bi_2Fe_4O_9$ does not contribute to measured magnetocapacitance of NCs with compositions $x=0.1$, 0.2.

F. Mössbauer spectroscopic studies

Distribution of iron atoms at the available sites and their chemical environment are investigated using Mössbauer spectroscopy. Fig. 8 shows room temperature Mössbauer spectra of all nanocomposites. Iron in SRF is present only as Fe^{3+} and is distributed into five crystallographically different sites denoted as 12 k, $4f_1$, $4f_2$, 2a, and 2b.[23] Out of these five sites, hyperfine parameters of $4f_1$ and 2a are nearly the same; hence, Mössbauer pattern of a pure SRF is fitted with four sextets. Mössbauer spectrum of 0.1SRF-0.9BFO NC has been fitted with five sextets and one doublet. Among these five sextets, four are assigned to different Fe^{3+} sites of SRF and the fifth one is due to Fe^{3+} sites of BFO. Distinction between iron sites of BFO and SRF is made from the values of different analyzed Mössbauer hyperfine parameters including isomer shift, quadrupole splitting, and internal hyperfine field and they are tabulated in Table III. The doublet denotes a paramagnetic phase of impure $Bi_2Fe_4O_9$. Mössbauer spectra of other composites ($x=0.2$, 0.3, and 0.4) have been fitted with five sextets attributed to both phases of SRF and BFO. It can be seen from the figure that there is no doublet in the central region of Mössbauer spectra for $x=0.2$, 0.3, and 0.4. This is due to dilution of the impure phase with increasing SRF content. These findings agree well with XRD results. Spectra of all nanocomposites reveal the presence of all crystallographic inequivalent Fe^{3+} ordered sites of both BFO and SRF phases confirming the formation of the composites.

IV. CONCLUSIONS

Nanocomposites (NCs) comprising $(1-x)$ BFO and x SRF have been synthesized by a sol-gel route, and their structural, dielectric, hyperfine, magnetic, and magnetoelectric properties are investigated. XRD analysis confirms the presence of pure phases of BFO and SRF in the NCs with $x = 0.3$ and 0.4. TEM measurements indicate crystalline nature of the constituents with average particle size of around 30 nm. Magnetization measurements indicate a ferrimagnetic behavior in all the NCs. Saturation magnetization value of the NCs was found to increase with the increase in SRF content. Dielectric constant (ε_r) of the NCs shows a dispersive behavior with frequency and decreases with increase of SRF content. ε_r-T graphs of the NCs show an anomaly around the antiferromagnetic transition temperature of BFO indicating the presence of magnetoelectric coupling. Magnetocapacitance of the NCs measured in the range of −110 to 110 kOe demonstrates the enhancement of magnetoelectric effect in the NCs with respect to the pristine BFO. ^{57}Fe Mössbauer analysis indicates that iron atoms are present as Fe^{3+} in the crystallographically inequivalent sites of BFO and SRF and all the sites are magnetically ordered.

ACKNOWLEDGMENTS

The authors acknowledge Mr. Binoy Krishna Hazra, School of Physics, University of Hyderabad, for high temperature dielectric measurements. The author A. Das is grateful to University Grants Commission (UGC), New Delhi, for providing the Senior Research Fellowship. The authors would like to thank Department of Science and Technology, India (Project No. IR/S2/PU-06/2006) for low temperature high magnetic field facility at UGC-DAE Consortium for Scientific Research, Kolkata Centre.

[1]K. F. Wang, J.-M. Liu, and Z. F. Ren, Adv. Phys. **58**, 321 (2009).
[2]N. A. Spaldin and M. Fiebig, Science **309**, 391 (2005).
[3]J. M. Caicedo, J. A. Zapata, M. E. Gómez, and P. Prieto, J. Appl. Phys. **103**, 07E306 (2008).
[4]G. S. Lotey and N. K. Verma, J. Nanopart. Res. **14**, 742 (2012).
[5]G. L. Song, H. X. Zhang, T. X. Wang, H. G. Yang, and F. G. Chang, J. Magn. Magn. Mater. **324**, 2121 (2012).
[6]Y.-K. Jun, W.-T. Moon, C.-M. Chang, H.-S. Kim, H. S. Ryu, J. W. Kim, K. H. Kim, and S.-H. Hong, Solid State Commun. **135**, 133 (2005).
[7]H. Singh and K. L. Yadav, J. Phys.: Condens. Matter **23**, 385901 (2011).
[8]C.-X. Li, B. Yang, S.-T. Zhang, R. Zhang, Y. Sun, H.-J. Zhang, and W.-W. Cao, J. Am. Ceram. Soc. **97**, 816 (2014).
[9]P. Uniyal and K. L. Yadav, J. Alloys Compd. **492**, 406 (2010).
[10]A. Das, A. Roychowdhury, S. P. Pati, S. Bandyopadhyay, and D. Das, AIP Conf. Proc. **1591**, 399 (2014).
[11]A. Das, A. Roychowdhury, S. P. Pati, S. Bandyopadhyay, and D. Das, Phys. Scr. **90**, 025802 (2015).
[12]L. Lutterotti, MAUD version 2.33, 2011, see http://www.ing.unitn.it/~maud.
[13]R. K. Mishra, D. K. Pradhan, R. N. P. Choudhary, and A. Banerjee, J. Magn. Magn. Mater. **320**, 2602 (2008).
[14]Reetu, A. Agarwal, S. Sanghi, Ashima, and N. Ahlawat, J. Phys. D: Appl. Phys. **45**, 165001 (2012).
[15]A. Kumar, K. L. Yadav, H. Singh, R. Pandu, and P. R. Reddy, Physica B **405**, 2362 (2010).
[16]S. N. Babu, J.-H. Hsu, Y. S. Chen, and J. G. Lin, J. Appl. Phys. **107**, 09D919 (2010).
[17]P. Uniyal and K. L. Yadav, J. Phys.: Condens. Matter **21**, 012205 (2009).
[18]Y. A. Chaudhari, C. M. Mahajan, P. P. Jagtap, and S. T. Bendre, J. Adv. Ceram. **2**, 135 (2013).
[19]R. K. Mishra, D. K. Pradhan, R. N. P. Choudhary, and A. Banerjee, J. Phys.: Condens. Matter **20**, 045218 (2008).
[20]M. J. Iqbal, M. N. Ashiq, and I. H. Gul, J. Magn. Magn. Mater. **322**, 1720 (2010).
[21]D. H. Wang, W. C. Goh, M. Ning, and C. K. Ong, Appl. Phys. Lett. **88**, 212907 (2006).
[22]V. R. Palkar, D. C. Kundaliya, S. K. Malik, and S. Bhattacharya, Phys. Rev. B **69**, 212102 (2004).
[23]G. K. Thompson and B. J. Evans, J. Appl. Phys. **73**, 6295 (1993).